Open Ceramics 22 (2025) 100795

Contents lists available at ScienceDirect

Open Ceramics

journal homepage: www.sciencedirect.com/journal/open-ceramics

Influence of calcination temperature on the physicochemical properties of atomic/molecular layer deposited hybrid inorganic/organic ceramic nanofiltration membranes

M.P. Nijboer [a], H. Sondhi [a], E. Makhoul [b], M. Bechelany [b,c], S. Gabrielli [d], F. Roozeboom [a], A. Nijmeijer [a], A.Y. Kovalgin [e], M.W.J. Luiten-Olieman [a,*]

[a] Inorganic Membranes, University of Twente, PO Box 217, 7500 AE Enschede, the Netherlands
[b] Institut Européen des Membranes, IEM, UMR-5635, Université Montpellier, ENSCM, CNRS, Place Eugène Bataillon, 34095 Montpellier, France
[c] Functional Materials Group, Gulf University for Science and Technology (GUST), Mubarak Al-Abdullah 32093, Kuwait
[d] School of Science & Technology - Chemistry Division, ChIP Building, Via Madonna delle Carceri, 62032, Camerino (MC) Italy
[e] Integrated Devices and Systems, University of Twente, PO Box 217, 7500 AE Enschede, the Netherlands

ARTICLE INFO

Keywords:
Hybrid atomic/molecular layer deposition
Ceramic nanofiltration (nf) membranes
Calcination temperature
Structural and physico-chemical properties
Tunable hydrophobicity

ABSTRACT

Post-deposition calcination in the air of hybrid inorganic/organic layers is considered to remove the organic constituents and completely create a full inorganic membrane. This study aims to investigate to what extent such a removal occurs and the effect of remaining organic constituents on the physicochemical properties of the membrane layer.

Three hybrid layers were deposited using trimethylaluminum, two aliphatic- (ethylene glycol and 1,6-hexanediol) and one aromatic alcohol (hydroquinone). The effects of the different calcination treatments on the physicochemical properties were investigated. Differential thermogravimetric analysis established that the maximum mass loss rate temperatures for the hybrid layers grown from the aliphatic alcohols are lower than those from the aromatic co-reactant. After 250 °C, water contact angles (WCAs) were between 46° - 92° and IR spectroscopy and XPS showed the presence of carbon. Calcination at 350 °C reduced the WCA to 0° - 25° and decreased carbon content.

1. Introduction

Membranes are becoming increasingly interesting for chemical separations as an electrically rather than a thermally driven process. While more expensive, ceramic nanofiltration (NF) membranes are more stable in challenging chemical conditions than polymeric membranes [1]. However, with state-of-the-art preparation methods such as sol-gel based technology, it is challenging to create pores with ~1 nm diameter and narrow size distribution in a reproducible way. Tight NF even requires pores well below 1 nm in diameter.

In this study, a combined system of Atomic Layer Deposition (ALD) and Molecular Layer Deposition (MLD) was chosen for the membrane modification. ALD is a well-established technique for controlling atomic-size layer thickness of inorganic thin films in microelectronics. MLD is an upcoming parallel technology using organic rather than inorganic vapors to grow thin organic films. The combination of ALD and MLD, in which an inorganic precursor reacts with an organic co-reactant, called hybrid inorganic-organic growth, is rapidly emerging as an innovative approach for creating custom-made metal-organic thin films [2,3]. Common inorganic precursors in ALD/MLD processes are diethyl zinc (DEZ), trimethylaluminum (TMA), and titanium tetrachloride ($TiCl_4$). In combination with these precursors, a plethora of co-reactants has been used, of which ethylene glycol (EG), 4,4′-oxydianiline (ODA), and hydroquinone (HQ) are reported on most often [3]. In thin film literature, materials with these compositions are commonly referred to as 'alucones', 'titanicones', or 'zincones', depending on the respective precursor metal atom [4–8].

Song et al. showed in 2016 that ALD/MLD made of $TiCl_4$-EG hybrid layers were through-porous after calcination [9]. For such a hybrid layer grown on anodized aluminum oxide (AAO) supports of 20 nm pore size, they reported a pure water permeability of 48 L/(m^2.h.bar) after calcination in air at 250 °C. Also, salt retentions of up to 43 % and methylene

* Corresponding author.
E-mail address: m.w.j.luiten@utwente.nl (M.W.J. Luiten-Olieman).

https://doi.org/10.1016/j.oceram.2025.100795
Received 27 February 2025; Received in revised form 25 April 2025; Accepted 12 May 2025
Available online 12 May 2025
2666-5395/© 2025 The Authors. Published by Elsevier Ltd on behalf of European Ceramic Society. This is an open access article under the CC BY-NC-ND license (http://creativecommons.org/licenses/by-nc-nd/4.0/).

blue retention values of up to 96 % were reported for this membrane. Correspondingly, Sengupta et al. [1] showed that the decomposition of a $TiCl_4$-EG hybrid layer in air starts after 250 °C. Wu et al. have further investigated a range of calcination temperatures from 250 °C - 500 °C [10]. They observed an increase in pure water permeability with an increase in calcination temperature, ascribing this effect to the volume shrinkage due to the crystallization occurring in the grains of the porous matrix. Usually, post-deposition calcination is considered to completely remove the organic constituents to create a full-inorganic membrane with reliably small pore size. Yet, we note the permeability increase upon calcination can also be related to the presence of non-decomposed organic constituents at the substrate surface. An in-depth study on the effect of the physicochemical properties of the co-reactant in combination with varying the post-deposition calcination temperature on the final membrane material is essential in developing the technique towards tailor-made membranes in terms of pore size, thermal stability, and hydrophilicity.

1.1. Scope

This study aims to explore the effect of the calcination temperature on the physicochemical properties (e.g., carbon presence and hydrophobicity) of three different 'alucone' hybrid layers in the temperature range where the significant mass loss of the organic constituent takes place. The layers were deposited on Al_2O_3-coated silicon samples and/or alumina ceramic supports. Trimethylaluminum was used as a precursor combined with two aliphatic alcohols (ethylene glycol, and 1,6-hexanediol), and one aromatic (hydroquinone) with a rigid backbone, as a co-reactant. After post-deposition calcination at 250 °C and 350 °C in air, the properties of the three different hybrid layers were studied and compared to those of the as-deposited hybrid layers.

2. Materials

2.1. Supports

Planar membrane (alpha-alumina; α-Al_2O_3) support discs of 21 mm in diameter and 2 mm in thickness, with a nominal pore diameter of 80 nm, were acquired from Pervatech B.V., The Netherlands [11]. Before use, the supports were sonicated in technical grade ethanol (Merck, The Netherlands) for 15 min, dried, and dip-coated with a gamma-alumina (γ-Al_2O_3) layer of 3 μm thickness with a nominal pore diameter of 10 nm. The sol used for dip-coating was doped with 3% v/v lanthanum nitrate solution. This procedure is described elsewhere in more detail [12]. The layer will be referred to as the La/γ-Al_2O_3 layer in the remainder of the article.

Silicon samples of 1 × 1 cm^2 were coated with a 10 nm layer of Al_2O_3 using ALD with trimethylaluminum and water as precursor and co-reactant to allow the subsequent ALD/MLD deposition to occur on an alumina surface coating rather than the native silicon oxide on a silicon sample. The process is described in more detail elsewhere [13].

Mesoporous aluminum oxide beads, as acquired from Saint-Gobain, France [14], were coated with the same 'alucone' films in the ALD-MLD reactor without any further pre-treatment and used as reference support in the TGA measurements.

2.2. Chemicals

Trimethyl aluminum (TMA, 97%), ethylene glycol (EG, 99%), 1,6-hexanediol (HD, 97%), and hydroquinone (HQ, 99%) were acquired from Sigma-Aldrich (France).

2.3. Reactor setup and reaction conditions

ALD/MLD was carried out in a home-built temporal reactor setup, described in more detail elsewhere [13,15]. The deposition parameters were optimized as described in a previous paper [16]; the temperature was kept constant at 150 °C for all precursor and co-reactant combinations. After placing the samples, the reactor was purged using argon gas and pumped for one hour before starting deposition. TMA, kept at room temperature, was pulsed for 0.4 s, followed by an exposure time of 10 s before being purged by argon dosed at 100 sccm for 30 s. The co-reactants were kept at elevated temperatures to achieve sufficient vapor pressure. These temperatures were based on values known from the literature. Details about the deposition parameters are listed in Table 1.

Samples were calcined in air directly after deposition in a Vecstar Ltd. XF chamber furnace at 250 °C and 350 °C, respectively for 3 hours, using heating and cooling rates of 1 °C/min.

2.4. Characterization methods

2.4.1. Spectroscopic ellipsometry

The thickness of the as-deposited MLD layers was determined on the Si wafer samples by ex-situ spectroscopic ellipsometry (SE). The measurements were performed on a J.A. Woollam M-2000X ellipsometer with a multi-chromatic light source and recorded in the spectral range of 210 to 1000 nm.

Fig. 1 illustrates a model describing the layers grown on top of planar silicon support to fit the data obtained by SE measurement. The three layers on top of the silicon support are a native silicon oxide layer (1 nm), an ALD-deposited Al_2O_3 layer (10 nm), and the top layer with an unknown layer thickness.

For the silicon support, the native silicon oxide as well as the ALD Al_2O_3 layer, the optical constants (n and k) are known from the J.A. Woollam database and can be used to fit the data. However, the optical constants for the ALD/MLD top layer cannot be taken from the J.A. Woollam database as its porosity, composition and optical constants are unknown. To account for the porosity of the hybrid layer, the model of the layer was converted to a so-called effective medium approximation (EMA) with a second constituent included, being voids [17]. At the same time, the optical constants were assumed to be those of pure α-Al_2O_3. The growth per cycle (GPC) was formally calculated by dividing the ALD/MLD layer thickness, thus obtained by the number of growth cycles [18].

2.4.2. Thermogravimetric analysis

Thermogravimetric Analysis (TGA) was used to assess the mass loss of the MLD layers upon heating with a TA Instruments SDT-Q600 tool. Analyses were performed by heating the sample in an air atmosphere from 25 to 800 °C at 10 °C/min. Differential thermal analysis (DTA) was conducted to identify the peak maximum of the mass loss rate curve.

2.4.3. High-resolution scanning electron microscopy

High-resolution scanning electron microscopy (HR-SEM, Zeiss Merlin system with a field emission source and a point resolution of 1.2 nm) was used for cross-section analyses of the hybrid layers. Layer thickness measurements were taken manually using the ImageJ Measure function at 20 locations for each sample after calcination.

Table 1
Overview of flask temperatures and pulse, exposure and purge durations for all co-reactants. The pulse, exposure, and purge times for TMA were constant at 0.4, 10, and 30 s, respectively.

Co-reactant	Temperature (°C)	Pulse time (s)	Exposure time (s)	Argon purge time (s)
Ethylene glycol (EG)	90	7	20	120
1,6-Hexanediol (HD)	85	7	10	60
Hydroquinone (HQ)	130	10	10	60

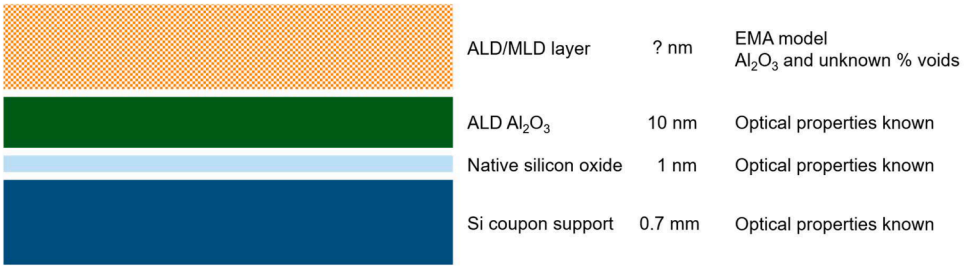

Fig. 1. Schematic of the model structure and assumed optical properties of the four layers considered in the model for spectroscopic ellipsometry.

2.4.4. X-ray photoelectron spectroscopy

X-ray photoelectron spectroscopy (XPS) measurements were performed using a PHI Quantes scanning XPS system (Nanolab, MESA+ Institute, Enschede, The Netherlands) to determine the carbon content of the materials in the form of a depth profile. XPS depth profiles were constructed by sequential sputtering using Ar^+ ions and XPS measurements of the silicon samples. The sputtering was performed at a 2 × 2 mm^2 raster size at 3 kV, resulting in a sputter rate of approximately 9.8 nm on SiO_2. More detailed specifics of the system and its operation were reported elsewhere [19].

2.4.5. Water contact angle

Water contact angle (WCA) measurements of the layers before and after calcination were performed with the sessile drop method using a DSA30S optical tensiometer from Krüss GmbH, Hamburg, Germany. The automated syringe needle deposited droplets of 3 μl Milli-Q water onto the sample surface. The contact angles were recorded immediately.

2.4.6. Fourier transform – infrared spectroscopy

Fourier Transform Infrared spectroscopy (FT-IR) with attenuated total reflection (ATR) was performed on a PerkinElmer Spectrum Two spectrometer to identify the covalent organic bonds present before and after calcination of the deposited layers. The measurements were recorded at a resolution of 0.2 cm^{-1} using 16 scans.

3. Results and discussion

3.1. Layer thickness measurements

The layer growth of the hybrid ALD/MLD layers during the deposition process can be affected by many parameters, e.g., the precursor and co-reactant combinations, substrate, deposition temperature, precursor dose, and purge time. To allow the deposition of layers with a similar layer thickness (~30 nm) on ceramic supports, the growth per cycle (GPC) of the different precursor and co-reactant combinations was determined on Al_2O_3-coated silicon samples using SE. The results are given in Table 2. The GPC values thus obtained were comparable to those reported in the literature: the combinations of TMA-EG and TMA-HD match closely [20–22]. The scarce GPC values reported in the literature for TMA-HQ film combinations are higher at 0.85 nm/cycle, compared to 0.15 nm/cycle in this work [21,23]. These results determined the definitive number of cycles for the different precursor and co-reactant combinations for depositions on membrane samples.

Table 2
As-deposited hybrid layer thicknesses measured on Al_2O_3-coated silicon samples using spectroscopic ellipsometry (SE) for 3 TMA - co-reactant combinations.

	Cycles on Al_2O_3-coated silicon (-)	Layer thickness (nm)	GPC (nm)	No. of cycles for final samples (-)
Ethylene glycol (EG)	200	110	0.55	65
1,6-Hexanediol (HD)	300	80	0.27	120
Hydroquinone (HQ)	300	44	0.15	225

In Fig. 2, TGA curves are depicted for the three hybrid layers deposited onto mesoporous alumina beads with increasing temperature, as well as the differential thermal analysis (DTA) curves. The different stages in mass loss in these hybrid layers indicate two crucial processes. In the first stage of the curve, from 25 °C up to 200 °C, mass is lost due to any unbound reactants' evaporation and physisorbed water's evaporation. The second stage of mass loss, between 200 °C and 450 °C, is characteristic of the oxidation of the organic constituents in the hybrid layer. The derivative mass loss curves are plotted in Fig. 1b, depicting the point of steepest mass loss. The temperatures corresponding to the maximum mass loss rate are 294 °C, 318 °C, and 366 °C for TMA-HD, TMA-EG, and TMA-HQ, respectively, indicating that more energy is required for the degradation of the hybrid layers with aromatic constituents than for the two hybrid layers with aliphatic constituents.

To investigate the effect of the maximum mass loss rate temperature on the layer thickness after calcination at 250 °C and 350 °C, c and TMA-HQ were chosen because they have the lowest and highest maximum mass loss rate temperatures (294 °C and 366 °C, resp.). HR-SEM imaging and SE were used to determine the layer thicknesses of two thin films grown on a planar Si substrate. The HR-SEM images in Fig. 3 show a uniform layer thickness for all four layers. Layer thicknesses were measured at 20 spots distributed over a cross-section of each sample, and their mean value and standard deviation were calculated as listed in Table 3. A layer thickness decrease was measured for TMA-HD (from 22 ± 3 to 16 ± 1 nm), while no significant reduction was measured for TMA-HQ (38 ± 4 nm and 42 ± 4 nm) after calcination at 250 °C and 350 °C, respectively. The difference might be related to the highest maximum mass loss rate temperature. For TMA-HD, the highest maximum mass loss rate temperature, 294 °C, is below the highest calcination temperature of 350 °C, while for TMA-HQ, 366 °C, is above the highest calcination temperature of 350 °C.

We note that the determination of layer thickness based on HR-SEM cross-section imaging has the intrinsic limitation of only showing a limited portion of a sample (a few hundred nanometers in our case).

The layer thicknesses were also routinely measured with SE. In the experimental part, a model is described to fit the data. The optical properties of Al_2O_3 were chosen as a basis, with uncertainty about the composition and porosity described by using an EMA in that layer of the model. The results are listed in the right-hand side columns of Table 3.

The layer thicknesses measured by SEM and SE of the TMA-HD layer are similar after the calcination step at 350 °C confirming the validity of the used SE model. The layer thickness after calcination of the TMA-HD layer at 250 °C is significantly lower when measured by SE as compared to SEM. This deviation could be caused by a substantial portion of the organic constituent still being present in the layer. The TGA showed that the maximum mass loss rate of the TMA-HD layer occurred at 294 °C. Similarly, in the case of TMA-HQ, the mass loss occurred at a higher temperature, indicating that most organic constituents will still be present in the hybrid top layer, even after calcination at 350 °C. As a result, the layer thicknesses as measured with SE deviate from those measured

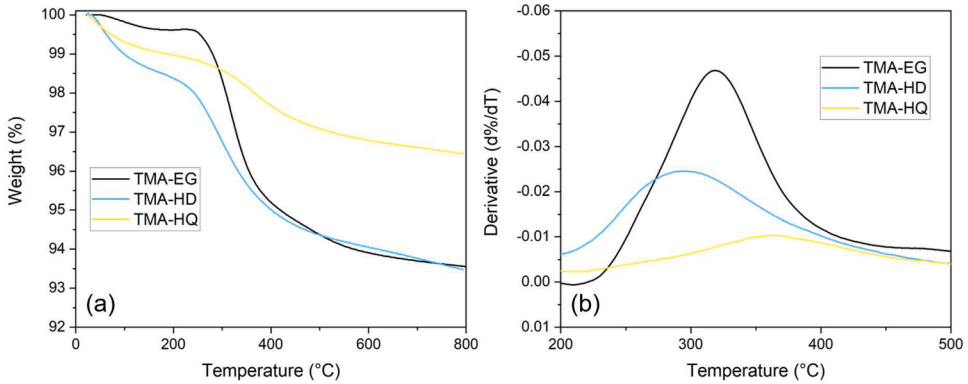

Fig. 2. (a) TGA curves for all three precursor and co-reactant combinations. It should be noted that the total weight refers to that of both the mesoporous alumina beads and the hybrid layer samples. (b) Derivative plots of the TGA curves indicate the highest mass loss rate point. EG = Ethylene glycol; HD = 1,6-Hexanediol; HQ = Hydroquinone.

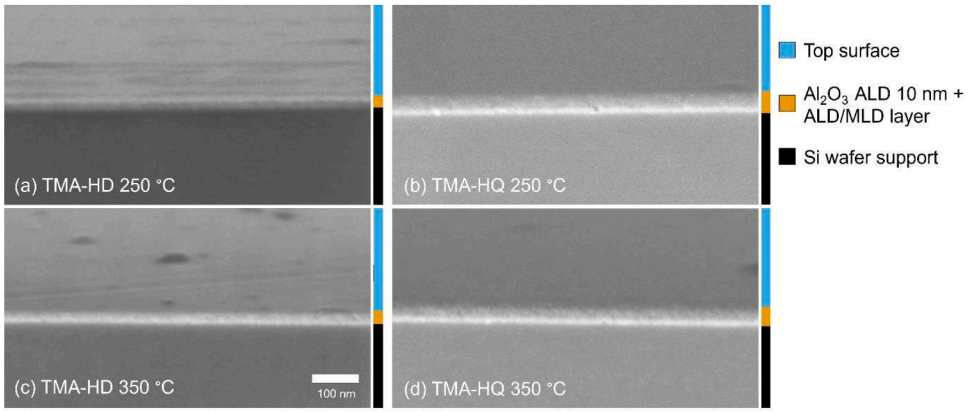

Fig. 3. Tilted HR-SEM micrographs of the layers after thermal treatment of TMA-HD at (a) 250 °C and at (c) 350 °C, and for TMA-HQ calcined at (b) 250 °C and at (d) 350 °C. HD = 1,6-Hexanediol; HQ = Hydroquinone. The orange-colored bars indicate the approximate thickness of the individual layers visible in the image.

Table 3
As measured by SEM and SE, layer thicknesses and the mean square error (MSE) values of each fit in SE.

	Calcination temperature (°C)	Average SEM layer thickness (nm)	SE layer thickness (nm)	MSE of SE fit (-)
TMA - HD	250	22 ± 3	15	10
	350	16 ± 1	15	10
TMA - HQ	250	38 ± 4	49	62
	350	42 ± 4	49	18

with SEM, likely because the SE model cannot consider the carbon. This is also reflected in the fit's high MSE values. The small apparent increase in layer thickness, measured by SEM and falling within the standard deviation of each other, of TMA-HQ with increasing calcination temperature, could be related to a small variation in the deposition phase of the hybrid layer. The SEM results furthermore highlight the difference between absolute layer thickness of the TMA-HD and TMA-HQ hybrid layers. This could result from the molecular structure of the two co-reactants during deposition. As mentioned earlier, the flexible chain of HD could result in double reactions, reducing the growth rate, whereas the rigid HQ molecule retains a higher growth rate during the deposition process.

3.2. X-ray photoelectron spectroscopy

To gain more insights into the distribution of carbon in the layer after calcination (XPS) depth profiles have been recorded for TMA-EG, as this is the most used in literature, and TMA-HQ, as this has the highest maximum mass loss rate temperature, on Al_2O_3-coated silicon substrates. The elemental depth profile graphs are shown in Fig. 4. The spectra of the TMA-EG layers after calcination at 250 °C and 350 °C are depicted in the top two plots, showing a sudden decrease in Al-signal coinciding with an increase in Si-signal after an etch time of 240 and 120 s for annealing at 250 °C and 350 °C, respectively. These changes indicate the breakthrough of the sputtering ion beam through the Al_2O_3-coating on the silicon support, pointing to a decrease in layer thickness after increasing the calcination temperature. Similar trends have been observed with SEM inspection; see above.

Looking at the depth profile for the TMA-HQ hybrid layer in the bottom row of Fig. 4, the sudden decrease in Al-signal coinciding with an increase in Si signal is visible after an etch time of 380 s for both samples TMA-HQ samples, calcined at 250 °C and 350 °C, respectively. Based on this observation, a similar layer thickness is expected for the layer calcined at 250 °C and 350 °C, assuming the sputter rate is similar for both materials. This has also been observed with SEM. Furthermore, it was corroborated by the literature, from which it is known that TMA-HQ is more stable, with its strong attraction between the aromatic rings, each containing six π-electrons that can suppress the decomposition of the hybrid TMA-HQ layer [24].

3.3. Water contact angle measurements

The residual organic species remaining in the hybrid ALD/MLD layer can also affect its physical and chemical properties. To examine this effect, the water contact angle (WCA) was measured on a deposited layer

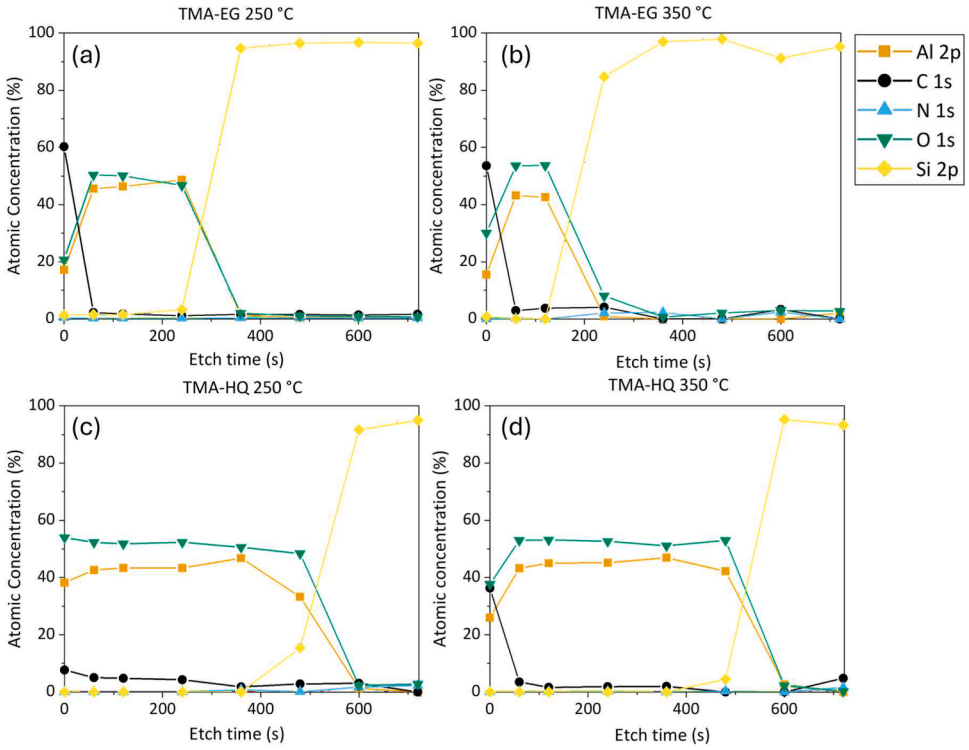

Fig. 4. XPS depth profiles of the TMA-EG layers (upper spectra) and for TMA-HQ (lower spectra). The layers were calcined at 250 °C and at 350 °C; see the insets. EG = ethylene glycol; HQ = Hydroquinone.

on an Al_2O_3-coated silicon sample and a γ-alumina membrane support. The TMA-HD layer was selected for this comparison, as its maximum mass loss peak in DTA is centered at 294 °C (see Fig. 1), i.e., equidistant of the two calcination temperatures. The water contact angle (WCA) values, were 76° and 77°, as measured directly after deposition on a planar Si substrate and an alumina membrane support, respectively. On the planar Si substrate, after calcination at 250 °C and 350 °C, the WCA of the TMA-HD layer, decreased from 76° to 39° and 11°, respectively. This is an expected trend as it is plausible that oxygen in the air will react with the organic species present in the hybrid layer during calcination, resulting in partial carbon removal at 250 °C. Increasing the temperature to 350 °C allows for a further increase in the reaction between air and organic compounds and, consequently, a further decrease in the WCA to 11° We note that on the membrane support, a different trend is observed for the TMA-HD hybrid layer; in this case, an increase in WCA is observed from 77° to 92° after calcination at 250 °C, after which it dropped to 0° upon the treatment at 350 °C. Directly after deposition, the WCA values of the hybrid layers on the two different support types were similar: the thin hybrid layer naturally covers the Al_2O_3-coated silicon sample surface. The hybrid layer forms a closed surface on top in the porous ceramic support, resulting in a similar WCA value between the two support types. During the calcination step, porosity is formed within the hybrid layer, increasing surface roughness [1]. From the literature, it is known that surface roughness (at length scales anywhere between unevenness in crystal lattices to the macroscopic 'flatness' of a surface) may enhance the intrinsic hydrophilic or hydrophobic properties of a material [25]; e.g. when a material is hydrophilic, the porosity enhances hydrophilicity and vice versa. The roughness and porosity of the membrane support can facilitate this effect. This phenomenon is better known for superhydrophobic materials as the lotus effect [26].

Table 4 gives an overview of the WCA values for the three precursor/co-reactant combinations after deposition and subsequent calcination at 250 °C and 350 °C. The WCA for as-deposited layers as compared to calcined layers (at 250 °C) increased for TMA-EG from 33° to 46°, and for TMA-HD from 77° to 92°, while for TMA-HQ (containing a benzene ring), no significant change in WCA is observed. After calcination in air at 350 °C, a significant decrease in WCA is observed for all three hybrid layers. This indicates that organic (carbon-containing), hydrophobic compounds in the surface layer have oxidatively dissociated to CO_2 at this annealing temperature, resulting in a more hydrophilic surface.

Table 4
Water Contact Angle of hybrid layers deposited on ceramic alumina supports. EG = Ethylene glycol; HD = 1,6-Hexanediol; HQ = Hydroquinone.

	After deposition (°)	250 °C (°)	350 °C (°)
TMA-EG	33	46	7
TMA-HD	77	92	0
TMA-HQ	88	82	25

3.4. Fourier transform infrared spectroscopy

Fourier transform infrared (FT-IR) analysis was performed to confirm the presence of carbon constituents in the layers, see Fig. 5. The spectrum of the pristine La/γ-Al_2O_3 layer is shown in Fig. 5a, showing a wide band positioned around 3400 cm^{-1}, which can be ascribed to -OH stretching vibrations. The band at 1640 cm^{-1} is characteristic of physisorbed water but can also be correlated to an -OH bending mode. The peak at 1500 cm^{-1} points to water deformation vibrations [27]. Characteristic of the Al-O stretching vibration in γ-alumina is the bands in between 500–700 cm^{-1} [28].

Fig. 5a also shows the FT-IR spectra of TMA-EG, TMA-HD, and TMA-HQ after deposition. These spectra show additional peaks between 2860–2970 cm^{-1}, indicating the asymmetric -CH, -CH_2, stretching of methylene groups [1,29]. Peaks are also visible between 1600–1000 cm^{-1}, pointing towards the presence of other functional groups with aromatic C—O in-plane vibrations (1225–1000 cm^{-1}), an intense methylene/methyl bending (1470 cm^{-1}) and a weak methylene bending (1380 cm^{-1}). Based on these spectra, the presence of carbon in the layers

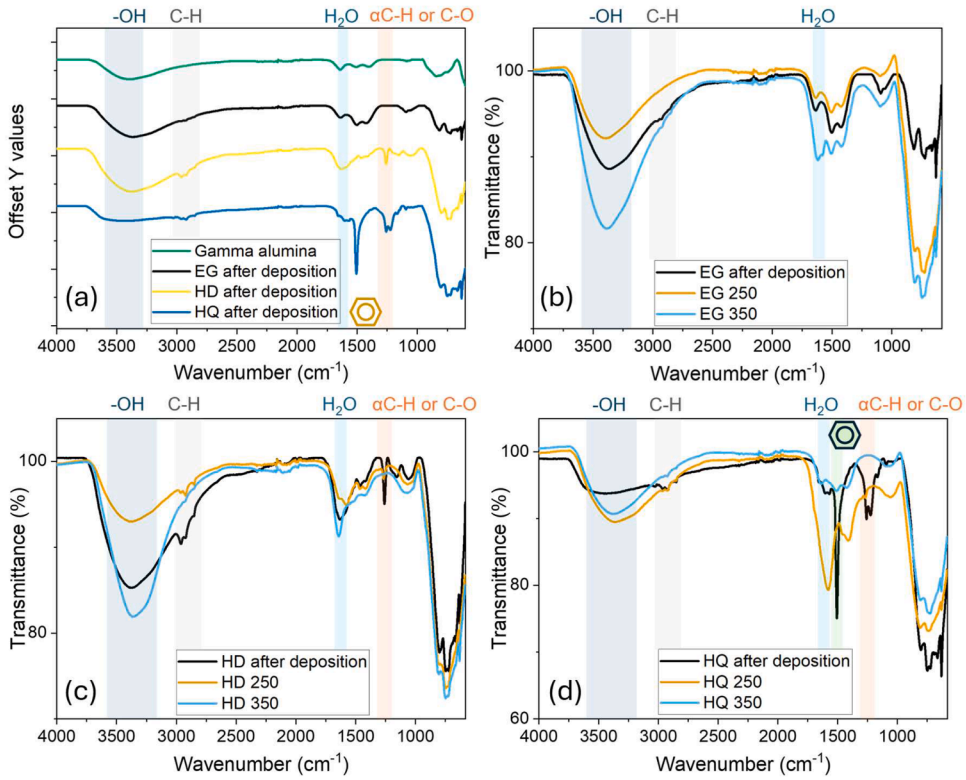

Fig. 5. Fourier Transform IR spectra of MLD-deposited alucone layers grown from TMA and the respective co-reactants. The spectra are given for the as-deposited layers and after calcination. Fig. 5a shows the spectra of the γ-alumina support and the layers after deposition. Figs. 5b-d show the spectra after deposition and after calcination at 250 °C and 350 °C for TMA-EG (EG = Ethylene glycol), TMA-HD (HD = 1,6-Hexanediol), and TMA-HQ (HQ = Hydroquinone), respectively. All spectra were baseline-corrected.

calcined at 250 °C was confirmed.

More importantly, FT-IR provides insight into the nature of the chemical bonds present in each layer and, subsequently, allows the monitoring of the progression of carbon loss by calcination. In general, Figs. 5b-d show that the vibrations at 2920–2850 cm^{-1} (indicative of -CH, -CH_2 stretching modes), the peaks at 1640 cm^{-1} (indicative of -OH bending of physisorbed water), and 1415 cm^{-1} (indicative of the -$C=C$ bending of unsaturated derivatives formed during calcination). For the layers of TMA-EG, and TMA-HD, (Fig. 5b-c), a similar decrease in intensity for carbon-related peaks and an increase in intensity for -OH-related peaks was observed with increasing annealing temperature. This aligns with the measured WCA, which drops to around 0° after calcination at 350 °C. The progression of these peaks confirms the increased carbon removal upon increasing calcination temperatures. TMA-HQ shows no significant increase in the intensity for -OH-related peaks, which can be correlated with the higher decomposition temperature as also observed with TGA-DTA, consequently, with the significantly higher WCA for this aromatic layer than the other aliphatic layers. A decrease in intensity for the aforementioned carbon-related bands is still visible.

4. Conclusions

We investigated the effect of calcination temperature on the structural and physicochemical properties of ALD/MLD deposited 'alucone' membrane layers by comparing as-deposited hybrid layers with post-deposition annealed layers. Three different hybrid layers were grown on Al_2O_3-coated silicon substrates and α-Al_2O_3 ceramic supports from TMA as an inorganic precursor, and three different organic co-reactants (ethylene glycol (EG), 1,6-hexanediol (HD), and hydroquinone (HQ)). TGA-DTA revealed that the temperatures at the respective maximum mass loss rates are lower for the two aliphatic alcohols used as a co-reactant (EG and HD) than that for the aromatic co-reactant (HQ), being 294 °C, 318 °C and 366 °C, respectively.

HR-SEM pictures showed that the point of maximum mass loss rate influenced the membrane layer's thickness at different calcination temperatures. Increasing the calcination temperature from 250 to 350 °C for the aliphatic co-reactant TMA-HD, with its maximum mass loss rate temperature of 318 °C, resulted in a significant decrease in apparent layer thickness from 22 to 16 nm. However, no significant decline in layer thickness was observed for the layer made with an aromatic co-reactant (TMA-HQ), with a maximum mass loss rate temperature of 366 °C.

The water contact angle (WCA) measurements showed an increase in the hydrophobicity for the TMA-EG and TMA-HD layers after calcination at 250 °C (from 33° to 49°, and 77° to 92°, respectively) while the WCA of TMA-HQ with its more stable benzene ring did not change and remained $> 80°$ Increasing the calcination temperature to 350 °C resulted in a significant decrease in WCA for the TMA-EG and TMA-HD layers to $< 10°$, and 25° in the case of TMA-HQ.

Fourier transform infrared spectroscopy (FT-IR) showed the presence of different functional organic bonds, indicating that partial degradation of the organic parts of the layers had occurred at a calcination temperature of 250 °C. A further increase to 350 °C showed a significant decrease in carbon-related signals in the FT-IR measurements and an increase in -OH-related peaks, thus showing a positive correlation between the carbon content and the hydrophobicity of the layers as described in the WCA results.

This work shows that the temperature in the calcination step and the choice of organic co-reactant significantly impact the carbon content in the final layer. This can be used to tune and optimize the hydrophobicity of ceramic nanofiltration membranes depending on the required pore size, affinity, and choice of starting chemicals.

Funding

This publication is part of the project "Waste to Feed; Sustainable treatment of challenging industrial (waste)streams with robust silicon carbide nano- or tight-ultrafiltration membranes (SUSSIC)" with project number 18,474 of the Open Technology research program which is partly financed by the Dutch Research Council (NWO).

CRediT authorship contribution statement

M.P. Nijboer: Writing – original draft, Visualization, Methodology, Investigation, Formal analysis, Conceptualization. **H. Sondhi:** Writing – review & editing, Methodology, Investigation. **E. Makhoul:** Writing – review & editing, Resources, Investigation. **M. Bechelany:** Writing – review & editing, Conceptualization. **S. Gabrielli:** Writing – review & editing, Formal analysis. **F. Roozeboom:** Writing – review & editing. **A. Nijmeijer:** Writing – review & editing. **A.Y. Kovalgin:** Writing – review & editing. **M.W.J. Luiten-Olieman:** Writing – review & editing, Funding acquisition, Conceptualization.

Declaration of competing interest

The authors declare that they have no known competing financial interests or personal relationships that could have appeared to influence the work reported in this paper.

Acknowledgements

The authors thank Kees van der Zouw for his help and guidance in interpreting the spectroscopic ellipsometry data. Mark Smithers is gratefully acknowledged for providing the HR-SEM images.

References

[1] B. Sengupta, Q. Dong, R. Khadka, D.K. Behera, R. Yang, J. Liu, J. Jiang, P. Keblinski, G. Belfort, M. Yu, Carbon-Doped Metal Oxide Interfacial Nanofilms for Ultrafast and Precise Separation of Molecules, Science 381 (2023) 1098–1104, https://doi.org/10.1126/science.adh2404.

[2] B.H. Lee, B. Yoon, A.I. Abdulagatov, R.A. Hall, S.M. George, Growth and Properties of Hybrid Organic-Inorganic Metalcone Films Using Molecular Layer Deposition Techniques, Adv Funct Mater 23 (2013) 532–546, https://doi.org/10.1002/adfm.201200370.

[3] J. Multia, M. Karppinen, Atomic/Molecular Layer Deposition for Designer's Functional Metal–Organic Materials, Adv Mater Interfaces 9 (2022) 2200210, https://doi.org/10.1002/admi.202200210.

[4] L. Ghazaryan, E.-B. Kley, A. Tünnermann, A. Viorica Szeghalmi, Stability and Annealing of Alucones and Alucone Alloys, J. Vac. Sci. Technol. A: Vac. Surf. Films 31 (2013) 01A149, https://doi.org/10.1116/1.4773296.

[5] H. Kim, J. Hyun, G. Kim, E. Lee, Y.S. Min, Origin of Instability of Titanicone Grown by Molecular Layer Deposition Using TiCl4 and Ethylene Glycol, Chem. Mater. 36 (2024) 247–255, https://doi.org/10.1021/acs.chemmater.3c02018.

[6] A. Philip, L. Mai, R. Ghiyasi, A. Devi, M. Karppinen, Low-Temperature ALD/MLD Growth of Alucone and Zincone Thin Films from Non-Pyrophoric Precursors, Dalton Trans. 51 (2022) 14508–14516, https://doi.org/10.1039/d2dt02279f.

[7] J. Liu, B. Yoon, E. Kuhlmann, M. Tian, J. Zhu, S.M. George, Y.C. Lee, R. Yang, Ultralow Thermal Conductivity of Atomic/Molecular Layer-Deposited Hybrid Organic-Inorganic Zincone Thin Films, Nano Lett 13 (2013) 5594–5599, https://doi.org/10.1021/nl403244s.

[8] X. Liang, A.W. Weimer, An Overview of Highly Porous Oxide Films with Tunable Thickness Prepared by Molecular Layer Deposition, Curr Opin Solid State Mater Sci 19 (2015) 115–125, https://doi.org/10.1016/j.cossms.2014.08.002.

[9] Z. Song, M. Fathizadeh, Y. Huang, K. Hoon, Y. Yoon, TiO2 Nanofiltration Membranes Prepared by Molecular Layer Deposition for Water Purification, J Memb Sci 510 (2016) 72–78, https://doi.org/10.1016/j.memsci.2016.03.011.

[10] S. Wu, Z. Wang, S. Xiong, Y. Wang, Tailoring TiO2 Membranes for Nanofiltration and Tight Ultrafiltration by Leveraging Molecular Layer Deposition and Crystallization, J Memb Sci 578 (2019) 149–155, https://doi.org/10.1016/j.memsci.2019.02.037.

[11] Pervatech, Available online: https://www.pervatech.nl/(accessed on 30 August 2024).

[12] A. Nijmeijer, PhD thesis, University of Twente: Enschede, The Netherlands, 1999.

[13] P. Abi Younes, S. Sayegh, A.A. Nada, M. Weber, I. Iatsunskyi, E. Coy, N. Abboud, M. Bechelany, Elaboration of Porous Alumina Nanofibers by Electrospinning and Molecular Layer Deposition for Organic Pollutant Removal, Colloids Surf Physicochem Eng Asp 628 (2021) 127274, https://doi.org/10.1016/j.colsurfa.2021.127274.

[14] Saint-Gobain, Available online: https://www.saint-gobain.com/fr (accessed on 30 August 2024).

[15] S. Sayegh, J.H. Lee, D.H. Yang, M. Weber, I. Iatsunskyi, E. Coy, A. Razzouk, S. S. Kim, M. Bechelany, Humidity-Resistant Gas Sensors Based on SnO2 Nanowires Coated with a Porous Alumina Nanomembrane by Molecular Layer Deposition, Sens Actuators B Chem 344 (2021) 130302, https://doi.org/10.1016/j.snb.2021.130302.

[16] H. Sondhi, M. Nijboer, E. Makhoul, A. Nijmeijer, F. Roozeboom, M. Bechelany, A. Kovalgin, M. Luiten-Olieman, Increasing Hydrophobicity of Ceramic Membranes by Post-Deposition Nitrogen Annealing of Molecular Layer Deposition Grown Hybrid Layers, Appl Surf Sci 683 (2025) 161790, https://doi.org/10.1016/j.apsusc.2024.161790.

[17] Y. Liu, J. Qiu, L. Liu, Applicability of the Effective Medium Approximation in the Ellipsometry of Randomly Micro-Rough Solid Surfaces, Opt Express 26 (2018) 16560, https://doi.org/10.1364/oe.26.016560.

[18] J.R. van Ommen, A. Goulas, R.L. Puurunen, *Atomic Layer Deposition*; Major Reference Works, John Wiley & Sons, Inc., 2021. ISBN 9780471238966.

[19] M. Nijboer, A. Jan, M. Chen, K. Batenburg, J. Peper, T. Aarnink, F. Roozeboom, A. Kovalgin, A. Nijmeijer, M. Luiten-Olieman, Tuning Nanopores in Tubular Ceramic Nanofiltration Membranes with Atmospheric-Pressure Atomic Layer Deposition: prospects for Pressure-Based In-Line Monitoring of Pore Narrowing, Separations 11 (2024) 24, https://doi.org/10.3390/separations11010024.

[20] X. Liang, M. Yu, J. Li, Y.B. Jiang, A.W. Weimer, Ultra-Thin Microporous-Mesoporous Metal Oxide Films Prepared by Molecular Layer Deposition (MLD), Chem. Commun. (2009) 7140–7142, https://doi.org/10.1039/b911888h.

[21] D.W. Choi, M. Yoo, H.M. Lee, J. Park, H.Y. Kim, J.S. Park, A Study on the Growth Behavior and Stability of Molecular Layer Deposited Alucone Films Using Diethylene Glycol and Trimethyl Aluminum Precursors, and the Enhancement of Diffusion Barrier Properties by Atomic Layer Deposited Al2O3 Capping, ACS Appl Mater Interfaces 8 (2016) 12263–12271, https://doi.org/10.1021/acsami.6b00762.

[22] Y.S. Park, H. Kim, B. Cho, C. Lee, S.E. Choi, M.M. Sung, J.S. Lee, Intramolecular and Intermolecular Interactions in Hybrid Organic-Inorganic Alucone Films Grown by Molecular Layer Deposition, ACS Appl Mater Interfaces 8 (2016) 17489–17498, https://doi.org/10.1021/acsami.6b01856.

[23] S. Lee, G.H. Baek, J.H. Lee, D.W. Choi, B. Shong, J.S. Park, Facile Fabrication of P-Type Al2O3 /Carbon Nanocomposite Films Using Molecular Layer Deposition, Appl Surf Sci 458 (2018) 864–871, https://doi.org/10.1016/j.apsusc.2018.07.158.

[24] D.B. Ninković, J.P. Blagojević Filipović, M.B. Hall, E.N. Brothers, S.D. Zarić, What Is Special about Aromatic-Aromatic Interactions? Signif. Attract. Large Horiz. Displac., ACS Cent Sci 6 (2020) 420–425, https://doi.org/10.1021/acscentsci.0c00005.

[25] Krüss Scientific, Roughness (Surface Roughness) Available online: https://www.kruss-scientific.com/en/know-how/glossary/roughness (accessed on 11 February 2024).

[26] B. Zhu, R. Ou, J. Liu, Y. Yang, S. Chen, G. Wei, Z. Zhang, Fabrication of Superhydrophobic Surfaces with Hierarchical Structure and Their Corrosion Resistance and Self-Cleaning Properties, Surf. Interfaces 28 (2022) 101608, https://doi.org/10.1016/j.surfin.2021.101608.

[27] A. Boumaza, L. Favaro, J. Lédion, G. Sattonnay, J.B. Brubach, P. Berthet, A. M. Huntz, P. Roy, R. Tétot, Transition Alumina Phases Induced by Heat Treatment of Boehmite: an X-Ray Diffraction and Infrared Spectroscopy Study, J Solid State Chem 182 (2009) 1171–1176, https://doi.org/10.1016/j.jssc.2009.02.006.

[28] B. Ludwig, Infrared Spectroscopy Studies of Aluminum Oxide and Metallic Aluminum Powders, Part II: adsorption Reactions of Organofunctional Silanes, Powders 1 (2022) 75–87, https://doi.org/10.3390/powders1020007.

[29] D. Choudhury, S.K. Sarkar, N. Mahuli, Molecular Layer Deposition of Alucone Films Using Trimethylaluminum and Hydroquinone, J. Vac. Sci. Technol. A: Vac. Surf. Films 33 (2015) 01A115, https://doi.org/10.1116/1.4900934.